Acta Pharmacologica Sinica

www.nature.com/aps

ARTICLE

Thioridazine protects against disturbed flow-induced atherosclerosis by inhibiting RhoA/YAP-mediated endothelial inflammation

Min-chun Jiang[1], Huan-yu Ding[1], Yu-hong Huang[1], Chak Kwong Cheng[2], Chi Wai Lau[1], Yin Xia[1], Xiao-qiang Yao[1], Li Wang[2] and Yu Huang[1,2]✉

Atherosclerotic diseases remain the leading cause of adult mortality and impose heavy burdens on health systems globally. Our previous study found that disturbed flow enhanced YAP activity to provoke endothelial activation and atherosclerosis, and targeting YAP alleviated endothelial inflammation and atherogenesis. Therefore, we established a luciferase reporter assay-based drug screening platform to seek out new YAP inhibitors for anti-atherosclerotic treatment. By screening the FDA-approved drug library, we identified that an anti-psychotic drug thioridazine markedly suppressed YAP activity in human endothelial cells. Thioridazine inhibited disturbed flow-induced endothelial inflammatory response in vivo and in vitro. We verified that the anti-inflammatory effects of thioridazine were mediated by inhibition of YAP. Thioridazine regulated YAP activity via restraining RhoA. Moreover, administration of thioridazine attenuated partial carotid ligation- and western diet-induced atherosclerosis in two mouse models. Overall, this work opens up the possibility of repurposing thioridazine for intervention of atherosclerotic diseases. This study also shed light on the underlying mechanisms that thioridazine inhibited endothelial activation and atherogenesis via repression of RhoA-YAP axis. As a new YAP inhibitor, thioridazine might need further investigation and development for the treatment of atherosclerotic diseases in clinical practice.

Keywords: atherosclerosis; endothelium; inflammation; disturbed flow; Yes-associated protein; thioridazine.

Acta Pharmacologica Sinica (2023) 44:1977–1988; https://doi.org/10.1038/s41401-023-01102-w

INTRODUCTION

The prevalence of cardiovascular diseases has been steadily rising over the decades, with one in three deaths attributed to cardiovascular diseases worldwide [1]. Atherosclerosis provokes a variety of cardiovascular complications, including aortas aneurysms, ischemic heart diseases, and stroke [2]. Atherosclerosis remains the leading cause of cardiovascular morbidity and imposes heavy burdens on health systems globally, underscoring an urgent need for more effective pharmacological therapeutics [1, 3].

Atherosclerosis is characterized by the abnormal buildup of fibro-fatty materials in the arterial walls [2]. Atherosclerotic plaques are primarily distributed in the curvatures and branches of the artery trees exposed to low and oscillatory shear stress [4]. Endothelial cells form the innermost layer of arteries called endothelium. Endothelial cells are constantly exposed to multiple biomechanical stimuli including shear stress generated from different flow patterns [5]. Laminar flow occurs in the straight arterial regions and confers athero-protective effects, whereas disturbed flow in the bifurcations and bends prompts the atheroprone inflammatory response of endothelium [6]. Disturbed flow upregulates the expression of the adhesion molecule and chemokines in endothelial cells and thus facilitates the migration, infiltration, and retention of immune cells to the endothelium [4, 7]. Therefore, targeting endothelial inflammation induced by disturbed flow or other atheroprone drivers can yield benefits against atherogenesis.

The Hippo pathway is a highly conserved signaling pathway that plays an essential role in organ size control and tissue regeneration [8]. The Hippo pathway is composed of a kinase cascade that regulates multiple cellular functions including cell proliferation and apoptosis, cell-cell adhesion, and contact-inhibition. Yes-associated protein (YAP) and transcriptional coactivator with a PDZ-binding domain (TAZ, or WWTR1) are the primary downstream effectors of the Hippo pathway [9]. The two paralogs lack a DNA-binding domain, and thereby when activated, they bind to other transcription factors including TEA domain transcription factors (TEADs) to initiate the expression of target genes [10]. YAP and TAZ are reported to be implicated in mechano-transduction, and they integrate mechanical signals to regulate diverse cellular processes [11]. Our previous study revealed that laminar shear stress inhibited endothelial activation and atherogenesis via the integrin-Gα13–RhoA-YAP/TAZ axis [12]. Similarly, Ping et al. found that laminar flow promoted YAP degradation through autophagy and SIRT1-mediated deacetylation and thereby protected blood vessels

[1]School of Biomedical Sciences, Faculty of Medicine, The Chinese University of Hong Kong, Hong Kong, China and [2]Department of Biomedical Sciences, City University of Hong Kong, Hong Kong, China
Correspondence: Yu Huang (yu.huang@cityu.edu.hk)
These authors contributed equally: Min-chun Jiang, Huan-yu Ding.

Received: 26 December 2022 Accepted: 27 April 2023
Published online: 22 May 2023

against atherosclerosis [13]. On the contrary, oscillatory shear stress was reported to activate YAP through integrin α5β1/c-Abl to aggravate endothelial inflammation and atherosclerosis [14]. These findings indicate that YAP holds promise as a therapeutic target against atherosclerosis. Therefore, we aim to search for drugs or compounds that inhibit YAP activity. Considering that identifying YAP inhibitors from FDA-approved drugs might markedly accelerate the drug development, we built up a luciferase reporter assay-based drug screening system to screen the FDA-approved drug library.

In this study, we identified the antipsychotic drug thioridazine as a potent YAP inhibitor. Thioridazines treatment suppressed disturbed flow-induced endothelial inflammatory response in vivo and in vitro. Moreover, administration of thioridazine exerted anti-atherosclerotic effects in two mouse atherosclerosis models. Our study also provides new insights into the underlying mechanisms that thioridazine inhibits RhoA to regulate YAP activity. This work opens up the possibility of repurposing thioridazine for the intervention of atherosclerotic diseases.

MATERIALS AND METHODS

Animals

Eight- to twelve-week-old male *ApoE*$^{-/-}$ mice were supplied from the Laboratory Animal Services Centre, The Chinese University of Hong Kong. All the experimental protocols on mice were approved by the Animal Experimentation Ethics Committee, The Chinese University of Hong Kong, and in compliance with the Guide for the Care and Use of Laboratory Animals. All animal experiments complied with the ARRIVE Guidelines [15]. The mice were housed in the Animal Holding Core, The Chinese University of Hong Kong, under controlled conditions (23 ± 1 °C, 55% ± 5% humidity and 12 h light: 12 h dark cycle) with *ad libitum* access to water and food pellets. All the mice were randomly assigned to control group and thioridazine group (oral gavage, 5 mg·kg^{-1}·d^{-1}; Sigma-Aldrich, MA, USA; T9025). The mice were fed an atherogenic diet rich in cholesterol (Research diet, NJ, USA, D12336). Partial ligation of carotid artery in ApoE KO mice was conducted as previously described [12, 16, 17]. The mice were anesthetized by intraperitoneal injection of a mixture of xylazine (5 mg/kg) and ketamine (100 mg/kg). To dissect carotid arteries and aortae, mice were euthanized by CO_2 inhalation.

Cell culture

HUVECs and THP-1 cells were purchased from ATCC. HUVECs were cultured in DMEM/F12 (Gibco, USA) with EC growth supplement (50 μg/mL, Sigma-Aldrich, MA, USA). HUVECs within passage seven were used for experiments. THP-1 cells were cultured in RPMI-1640 medium (Gibco, USA). Culture media were supplemented with 10% fetal bovine serum (FBS; Gibco, USA) and 1% penicillin-streptomycin (Gibco, USA). All the cells were maintained in a humidified incubator at 37 °C with 5% CO_2. For HUVECs, electroporation was performed using the Basic Nucleofector Kit (Lonza, USA, VAPI-1001) for plasmid transfection. For hemodynamic study, HUVECs were seeded on fibronectin-coated glass slides (75 mm × 38 mm; Corning, USA). As previously described [12, 18], ibidi flow system (ibidi, Germany) and custom-built flow chambers were adopted to generate oscillatory shear stress (OSS, 0.05 ± 0.4 Pa, 1 Hz) for in vitro experiments on HUVECs.

CCK-8 assay

HUVECs (1×10^4) were seeded into each well of a 96-well culture plate and incubated overnight. Then the cells were treated with thioridazine at a range of concentrations for 24 h. Upon thioridazine treatment, 10 μL of Cell Counting Kit-8 (CCK-8, MCE, NJ, USA, HY-K0301) reagent was added to each well and incubated for another 4 h. The OD_{450} was measured by a microplate spectrophotometer (BIO-RAD, CA, USA).

Cell adhesion assay

HUVECs were seeded on glass slides (Corning, USA) and pretreated with thioridazine or vehicle for 4 h. Then the cells were subjected to OSS stimulation or kept static for 6 h. THP-1 cells were labeled with 1 μM Calcein-AM (Thermo Fisher Scientific, USA) for 30 min and then washed with PBS. THP-1 cells (5×10^5) were added to the HUVECs and co-incubated for one hour in a 37 °C incubator. Nonadherent THP-1 cells were washed away with fresh DMEM/F12 medium. The number of adhered THP-1 cells was counted under a fluorescence microscope.

Dual-luciferase reporter assay

8 × GTIIC firefly luciferase reporter plasmid (addgene #34615) and Renilla plasmid (addgene #118016) were simultaneously overexpressed in HUVEC by electroporation, and the cells were plated in 24-well or 96-well plates. After overnight culture, the cells were treated with different concentrations of thioridazine. After 24 h, activities of firefly and Renilla luciferase were detected by Dual-Luciferase Reporter Assay System (Promega, USA). To avoid errors from transfection efficiency variance, the results were expressed as the ratio of firefly luciferase to Renilla luciferase activity. TED-347 (HY-125269) was provided by MedChemExpress (NJ, USA). The FDA-approved drug library was purchased from Selleckchem (# L1300). For drug screening, 2×10^4 cells were seeded in each well of 96-well plates. Cells were treated with each compound at 10 μM for 24 h prior to the luciferase reporter assay.

Western blotting

Total proteins were extracted from HUVECs and mouse tissues using RIPA lysate (Beyotime, China) supplemented with cOmplete™ protease inhibitor cocktail (Roche, Switzerland) and phosSTOP™ phosphatase inhibitor cocktail (Roche, Switzerland). The protein concentration was quantitated by the Pierce BCA Protein Assay Kit (Thermo Fisher Scientific, USA). Equal amounts of proteins were separated by 8%–12% SDS-PAGE, and then transferred to PVDF membrane. After blocking with 3% BSA at room temperature, the membranes were incubated with primary antibodies overnight at 4 °C and then with corresponding HRP-conjugated secondary antibodies for 1 h at room temperature. Subsequently, the bands were visualized on the Bio-Rad ChemiDoc MP Imaging System using the enhanced chemiluminescence reagent (Millipore, USA). Quantitative analysis of band intensities was performed using ImageJ software. Primary antibodies used in this study include rabbit anti-GAPDH (Cell Signaling Technology, 2118), rabbit anti-YAP (Cell Signaling Technology, 14074), rabbit anti-phospho-YAP (Ser127) (Cell Signaling Technology, 4911), rabbit anti-RhoA (Abcam, ab187027) and mouse anti-β-tubulin (Transgen, HC101-01).

Active RhoA detection

The levels of active RhoA were determined by RhoA Pull-Down Activation Assay Biochem Kit (Cytoskeleton, USA). Briefly, cells were lysed in lysis buffer supplemented with protease inhibitor cocktail. After centrifugation at 10,000 × *g* for 5 min at 4 °C, equivalent protein amounts of lysates were incubated with rhotekin-RBD beads on a rotator at 4 °C for 1 h. The mixture then was centrifuged at 3000 × *g* for 1 min at 4 °C, and the supernatant was carefully removed, while the pellet was gently washed with wash buffer and centrifuged again at 3000 × *g* for 3 min at 4 °C. After removing the supernatant, 2× SDS loading buffers were added to the samples and boiled for 2 min. The level of active RhoA was analyzed using SDS-PAGE.

Immunofluorescence staining

HUVECs and carotid arteries were fixed with 4% PFA for 15 min. After permeabilization with 0.1% Triton X-100, the cells/the samples were blocked with 5% BSA for 2 h at room temperature, followed by incubation at 4 °C with primary antibodies: rabbit anti-

Table 1. Primer sequence for real-time PCR.

Species	Gene	Forward primer (5′-3′)	Reverse primer (5′-3′)
Human	*GAPDH*	TTCGTCATGGGTGTGAACCA	TGATGGCATGGACTGTGGTC
	ANKRD1	AGAACTGTGCTGGGAAGACG	GCCATGCCTTCAAAATGCCA
	CTGF	ACCGACTGGAAGACACGTTTG	CCAGGTCAGCTTCGCAAGG
	CYR61	TGAAGCGGCTCCCTGTTTT	CGGGTTTCTTTCACAAGGCG
	CXCL1	CTGGCTTAGAACAAAGGGGCT	TAAAGGTAGCCCTTGTTTCCCC
	IL-1β	AGCTACGAATCTCCGACCAC	CGTTATCCCATGTGTCGAAGAA
	IL-6	CCTGAACCTTCCAAAGATGGC	TTCACCAGGCAAGTCTCCTCA
	IL-8	TTTTGCCAAGGAGTGCTAAAGA	AACCCTCTGCACCCAGTTTTC
	MCP-1	CAGCCAGATGCAATCAATGCC	TGGAATCCTGAACCCACTTCT
	SELE	TGTGGGTCTGGGTAGGAACC	AGCTGTGTAGCATAGGGCAAG
	VCAM-1	CAGTAAGGCAGGCTGTAAAAGA	TGGAGCTGGTAGACCCTCG
Mouse	*Gapdh*	ACAGTCCATGCCATCACTGCC	GCCTGCTTCACCACCTTCTTG
	Ankrd1	GCTGGTAACAGGCAAAAAGAAC	CCTCTCGCAGTTTCTCGCT
	Ctgf	TCAACCTCAGACACTGGTTTCG	TAGAGCAGGTCTGTCTGCAAGC
	Cyr61	GCCGTGGGCTGCATTCCTCT	GCGGTTCGGTGCCAAAGACAGG
	Cxcl1	CTGGGATTCACCTCAAGAACATC	CAGGGTCAAGGCAAGCCTC
	Il-1β	GCAACTGTTCCTGAACTCAACT	ATCTTTTGGGGTCCGTCAACT
	Il-6	TAGTCCTTCCTACCCCAATTTCC	TTGGTCCTTAGCCACTCCTTC
	Il-8	TCGAGACCATTTACTGCAACAG	CATTGCCGGTGGAAATTCCTT
	Mcp-1	TTAAAAACCTGGATCGGAACCAA	GCATTAGCTTCAGATTTACGGGT
	Sele	ATGCCTCGCGCTTTCTCTC	GTAGTCCCGCTGACAGTATGC
	Vcam-1	AGTTGGGGATTCGGTTGTTCT	CCCCTCATTCCTTACCACCC

YAP (1:200; Cell Signaling Technology, 14074), Rabbit anti-VCAM1 (1:200; Abcam, ab134047) and Goat anti-VE-cadherin (1:300; Santa Cruz Biotechnology, sc-6458). The Alexa Fluor™ 546 (Thermo Fisher Scientific, A10040) and Alexa Fluor™ 488 (Thermo Fisher Scientific, A11055) secondary antibodies were used at 1:200 dilutions for incubation at room temperature for 2 h. The nuclei were stained with Hoechst 33342 for 15 min and mounted with anti-fade mounting media. Images were taken by TCS SP8 inverted confocal microscope (Leica, Germany).

Oil Red O staining

The mouse hearts and carotid arteries were dissected upon euthanasia and fixed in 4% PFA overnight. After three washes with PBS, the hearts and carotid arteries were hydrated in 30% sucrose solutions for 24 h and then were stored at −80 °C after embedding in optimum cutting temperature compound (OCT; Sakura Finetek, the Netherlands). The specimens were cut into 5 μm sections using a cryostat (Thermo Fisher Scientific, USA) for later H&E and Oil Red O staining. For *en face* staining, the mouse aortae were dissected longitudinally and fixed overnight in 4% PFA. The frozen sections and aortae were rinsed in water for 5 min and then in 60% isopropanol for 2 min. The samples were immersed in fresh Oil Red O solutions for 15 min, and then washed in 60% isopropanol for 2 min. The nuclei were counter-stained in alum haematoxylin for 1 min. After washing in water, the stained aortae were fixed on microscope slides. The sections and aortae were mounted with Glycerol Jelly Mounting Medium. Images were taken with a Nikon Ni-U Eclipse Upright Microscope (Nikon, Tokyo, Japan). Plaque proportions were analyzed using ImageJ software.

Quantitative RT-PCR

Total RNA was extracted from HUVECs and mouse tissues with TRIzol reagent (Takara, Japan). The RNA samples were reverse transcribed into cDNA using reverse transcriptase (Takara, Japan). cDNA was amplified by SYBR Green PCR Master Mix in ViiA^{TM} 7 real-time PCR system (Applied Biosystems, USA). The mRNA levels of genes were determined by the $2^{-\Delta\Delta CT}$ method, and GAPDH was an internal control. The primer sequences used in this study were listed in Table 1.

RNA sequencing and RNA-Seq data analysis

Total RNA was extracted according to the manual of RNeasy Mini Kit (Qiagen, Germany). RNA samples were sent to Wenzheng Biotechnology Co., Ltd. (Shenzhen, China) for RNA sequencing. Differentially expressed gene (DEG) analysis of thioridazine and control samples was performed by using DESeq2 (v1.34.0). $|\log2(\text{Fold change})| > 1$ and adjusted P-value < 0.05 were used as the cut-off value of differential genes. Gene Ontology (GO), Kyoto Encyclopedia of Genes and Genomes (KEGG), and GAD disease enrichment analysis were performed using DAVID tools.

Blood lipid profile

Venous blood was collected from the right ventricle immediately upon CO_2 euthanasia of mice. After centrifugation at 3000 r/min for 10 min at 4 °C, the supernatant serum was collected and stored at −80 °C. The commercial assay kit (Stanbio, USA) was used to detect the levels of total cholesterol, triglyceride, and HDL; non-HDL was calculated with the following formula: non-HDL cholesterol = TC-HDL-(TG/5).

Statistical analysis

All data were presented as mean ± standard error (mean ± SEM). For normally distributed data, unpaired Student *t*-test was performed for comparison between two groups (Welch correction was performed when the variance was unequal); One-way analysis of variance (ANOVA) with *post-hoc* Tukey test was used for comparison between multiple groups. As for data following a non-normal distribution, statistical analysis was conducted by using the Mann-Whitney U test for comparison between two groups, and Kruskal-Wallis test followed by Dunn multiple comparison test was used for comparison between multiple groups. Statistical

analysis was performed using GraphPad Prism 7. $P < 0.05$ was considered statistically significant.

RESULTS

Thioridazine was identified as a new YAP inhibitor by screening an FDA-approved drug library

We previously found that disturbed flow activated YAP/TAZ to boost endothelial inflammation. Endothelial YAP is a potential therapeutic target for anti-atherosclerotic treatment [12, 19]. To seek out new YAP inhibitors, luciferase reporter assay was employed to screen small-molecule compounds from an FDA drug library (Fig. 1a). HUVECs were transfected with YAP/TAZ-responsive luciferase plasmid, the promoter of which contains eight repeated TEAD-DNA binding motifs (8× GTIIC). TEA-347 served as a positive control. The antipsychotic drug thioridazine (10 μM) was identified to inhibit YAP activity in endothelial cells (Fig. 1b, Supplementary Fig. S1). Meanwhile, CCK-8 assay showed that thioridazine at 10 μM had no obvious toxic effects on the cell viability of HUVECs (Fig. 1c). Thioridazine suppressed the expression of YAP/TAZ target genes (*ANKRD1, CTGF, CYR61*) (Fig. 1d) and elevated YAP phosphorylation at Serine 127 (Fig. 1e, g) in a concentration-dependent manner in HUVECs. In addition, HUVECs treated with 10 μM of thioridazine showed a time-dependent increase of YAP phosphorylation (Fig. 1f, h). Consistently, Western blotting and immunofluorescence confirmed that thioridazine blocked YAP nuclear localization in HUVECs (Fig. 1i–k). Collectively, thioridazine promoted YAP^{S127} phosphorylation to constrain its activity.

RNA-seq analysis of the transcriptomic profile of thioridazine-treated endothelial cells

To further explore how thioridazine affected HUVECs, we isolated the total RNA of thioridazine-treated HUVECS for RNA-sequencing. The RNA-seq data analysis identified 1161 differentially expressed genes by setting the threshold as adjusted $P < 0.05$, $|\log_2(\text{Fold change})| > 1$ (Fig. 2a). KEGG enrichment analysis confirmed that thioridazine regulated the Hippo pathway in endothelial cells (Fig. 2b). Moreover, GO and GSEA analysis revealed that thioridazine treatment was associated with mechanical stimuli and endothelial activation (Fig. 2c, d). GAD disease analysis unveiled that the differentially expressed genes were significantly associated with cardiovascular diseases including atherosclerosis, indicating that thioridazine could be repurposed as an anti-atherosclerotic drug (Fig. 2e, f). Taken together, RNA-seq analysis provided clues that thioridazine might protect endothelium against biomechanical stimuli-induced inflammation and atherogenesis.

Thioridazine suppressed disturbed flow-induced endothelial inflammation via repression of YAP activity

To investigate whether thioridazine inhibited mechanical stimuli-induced endothelial activation, we performed partial ligation of carotid arteries to induce disturbed flow in ApoE KO mice (Fig. 3a). *En face* immunofluorescence staining of the ligated left carotid arteries showed that administration of thioridazine inhibited the expression of VCAM-1 in endothelium exposed to disturbed flow (Fig. 3b). Meanwhile, we applied the ibidi system to mimic disturbed flow for in vitro experiments (Fig. 3c). Thioridazine significantly suppressed OSS-induced expression of pro-inflammatory genes (*CXCL1, IL-1β, IL-6, IL-8, MCP-1, SELE, VCAM-1*) in HUVECs. (Fig. 3d). Consistently, monocyte adhesion assay suggested that thioridazine markedly impeded OSS-induced monocyte attachment to endothelial cells (Fig. 3e, f). To further explore whether thioridazine inhibited endothelial activation via repression of YAP, we transfected HUVECs with constitutively active YAP (CA-YAP). Then the HUVECs were subjected to thioridazine and OSS. As shown in Fig. 3g and Supplementary Fig. S2a, overexpression of CA-YAP reversed the anti-inflammatory effects of thioridazine in HUVECs exposed to disturbed flow. Therefore, thioridazine suppressed disturbed flow-induced endothelial inflammation primarily through YAP inhibition.

Thioridazine inhibited RhoA to promote YAP^{S127} phosphorylation

Previous studies reported that extracellular stimuli, such as shear stress, regulated YAP activity via the small GTPase RhoA [12, 20–22]. In line with the previous findings, GO analysis of RNA-seq data implied that thioridazine treatment was involved in the regulation of GTPase activity (Fig. 2c). Interestingly, we also observed morphological changes in HUEVCs treated with thioridazine. F-actin staining verified that thioridazine regulated cytoskeletal actin dynamics (Fig. 4a). Hence, we hypothesized that RhoA might be involved in the upregulation of YAP phosphorylation at Ser 127 induced by thioridazine. GST-RBD pull-down assay confirmed that thioridazine inhibited the activity of RhoA in HUVECs (Fig. 4b, c). To examine whether thioridazine increased YAP phosphorylation (Ser127) via inhibition of RhoA, we transfected HUVECs with constitutively active RhoA (Q63L). Western blotting analysis showed that overexpression of RhoA (Q63L) abrogated thioridazine-induced phosphorylation of YAP (Fig. 4g, h, Supplementary Fig. S2b, c). In accordance, quantitative PCR data indicated that CA-RhoA ablated the inhibitory effects of thioridazine on the expression of YAP target genes (*ANKRD1, CTGF, CYR61*) (Fig. 4d–f). Taken together, these data suggest that thioridazine upregulated YAP^{S127} phosphorylation via restraining RhoA activity.

Thioridazine mitigated partial ligation induced-atherogenesis in $ApoE^{-/-}$ mice

Partial ligation mouse model is commonly used for flow pattern-related atherosclerosis studies [16]. To determine the in vivo effects of thioridazine, we also applied the partial ligation mouse model to induce disturbed flow (Figs. 3a, 5b). Vehicle or thioridazine was administered to the $ApoE^{-/-}$ mice for three weeks (Fig. 5a). As shown in Fig. 5c, d, thioridazine alleviated atherogenesis in these mice received carotid partial ligation. Consistently, H&E and Oil Red O staining of the ligated LCA verified the anti-atherosclerotic effects of thioridazine (Fig. 5e–h). Furthermore, thioridazine inhibited RhoA and YAP activity (Fig. 5i, j, Supplementary Fig. S3a, b). Thioridazine suppressed the expression of YAP target genes and pro-inflammatory markers in aortae from $ApoE^{-/-}$ mice (Fig. 5k, l).

Thioridazine attenuated high cholesterol diet-induced atherosclerosis in $ApoE^{-/-}$ mice

To further examine the effect of thioridazine, we used another mouse model in which atherosclerosis was primarily attributed to high-cholesterol diet-triggered hyperlipidemia (Fig. 6a) [23]. $ApoE^{-/-}$ mice subjected to the vehicle or thioridazine (5 $mg \cdot kg^{-1} \cdot d^{-1}$) were fed an atherogenic diet for 12 weeks. *En face* Oil Red O staining verified that thioridazine retarded the plaque formation in the aortae of $ApoE^{-/-}$ mice (Fig. 6b, c). In line with results on the *en face* staining of aortae, H&E and Oil Red O staining of the aortic roots showed that thioridazine treatment diminished the plaque areas, compared with the control group (Fig. 6e–h). Immunofluorescent staining of F4/80 demonstrated that thioridazine reduced macrophage infiltration to the aortae (Fig. 6d). Notably, thioridazine did not cause alterations to lipid profiles (Fig. 6i) and body weights (Fig. 6j), implying that the anti-atherosclerotic effects of thioridazine are lipid-independent.

DISCUSSION

The present study is the first to identify the antipsychotic drug thioridazine as a novel YAP inhibitor through screening the FDA-approved drug library. In this study, we found that thioridazine upregulated YAP (Ser127) phosphorylation, thereby impeding its nuclear translocation and the initiation of the expression of its target genes and inflammatory genes. We further unveiled that thioridazine regulated cytoskeletal dynamics, and inhibited RhoA to

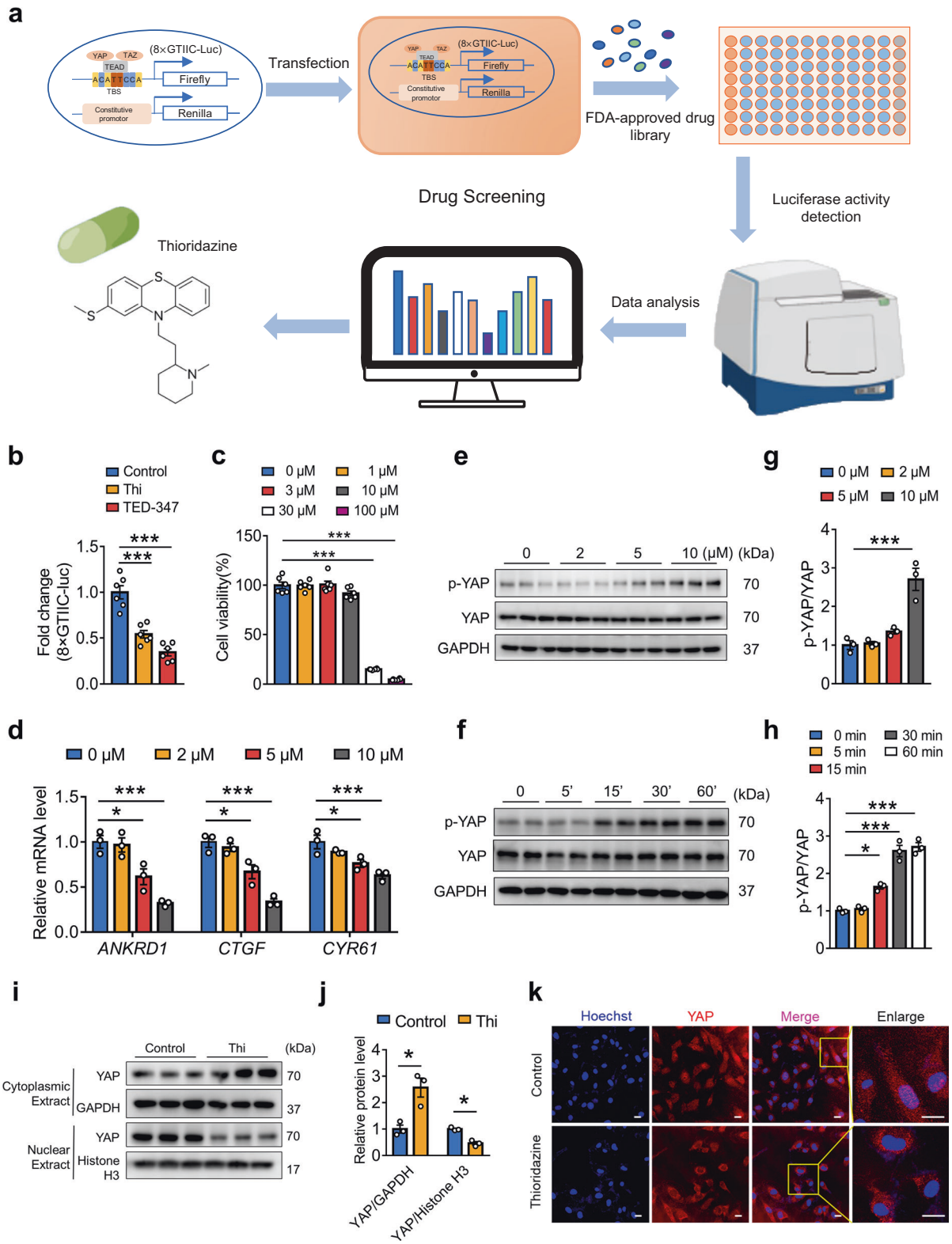

Fig. 1 Screening the new YAP inhibitor thioridazine from an FDA-approved drug library. a Diagram of drug screening system. **b** Luciferase reporter assay showed that thioridazine (10 μM) inhibited YAP/TAZ (8× GTIIC-Luc reporter gene) activity. TEA-347 served as a positive control ($n = 6$). **c** Cell viability assays of HUVECs in response to thioridazine treatment for 24 h were measured with CCK-8 kit ($n = 6$). **d**, **e** HUVECs were treated with different concentrations of thioridazine for 30 min and 4 h, respectively. **d** qRT-PCR results of the mRNA levels of YAP target genes. **e** Western blotting on the protein levels of p-YAP (Ser127) and total YAP. **f** Western blotting on the expression of p-YAP and total YAP in HUVECs treated with 10 μM of thioridazine at different time points. **g**, **h** Quantification of p-YAP level normalized to total YAP in **e**, **f** ($n = 3$). **i**, **j** HUVECs were treated with 10 μM of thioridazine for 1 h. Western blotting analysis of YAP distribution in nucleus and cytoplasm. **k** Immunofluorescence staining showing YAP cytoplasmic translocation in HUVECs, scale bar = 20 μm ($n = 3$). Data were presented as mean ± SEM. *$P < 0.05$, **$P < 0.01$, ***$P < 0.001$, vs control group.

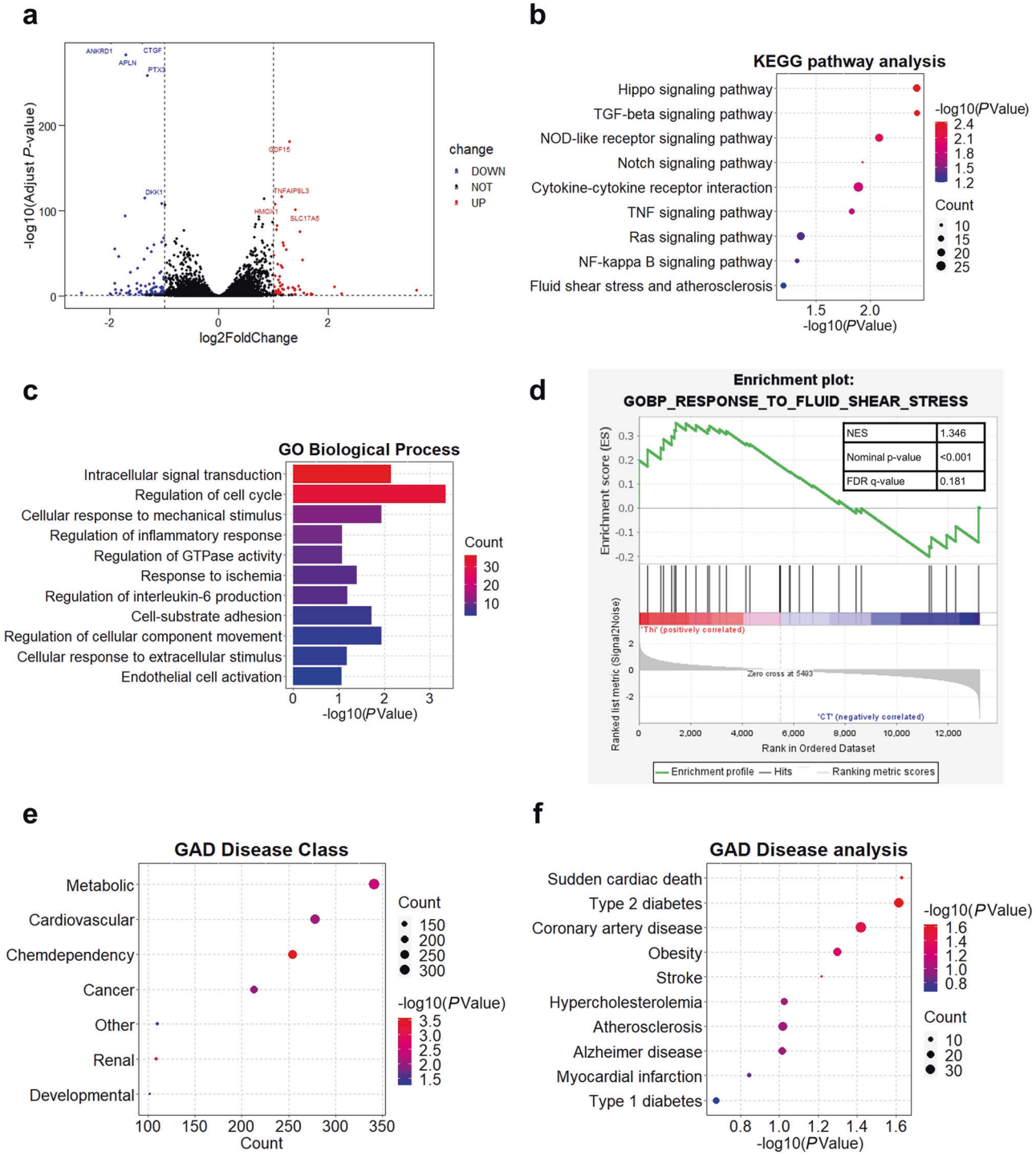

Fig. 2 RNA-seq analysis of the transcript profile of thioridazine-treated ECs. HUVECs were subjected to thioridazine treatment (10 μM) for 4 h. Total RNA was isolated for RNA sequencing. Comparative RNA-seq analysis was performed (thioridazine group versus control group, $n = 3$ per group). **a** Volcano plot demonstrating differentially expressed genes including 652 upregulated and 509 downregulated genes identified by using the threshold of adjusted $P < 0.05$, $|\log_2(\text{Fold change})| > 1$. **b** KEGG analysis. **c** GO analysis. **d** GSEA analysis. **e**–**f** GAD disease enrichment analysis.

promote phosphorylation of YAP^{S127}. Disturbed flow is one of the crucial contributors to endothelial inflammation and atherogenesis. In vivo and in vitro experiments verified that thioridazine suppressed disturbed flow-induced endothelial inflammation. More importantly, administration of thioridazine attenuated disturbed flow- and high-cholesterol diet-induced atherosclerosis in $ApoE^{-/-}$ mouse models, suggesting that repurposing thioridazine is a promising therapeutic strategy for atherosclerotic vascular diseases (Fig. 7).

As the leading cause of global death, atherosclerosis is a significant public health issue worldwide [1]. The first-line lipid-lowering medications statins have been used in many patients. However, some patients on long-term statins still develop atherosclerotic cardiovascular disease and even acute myocardial infarction [24].

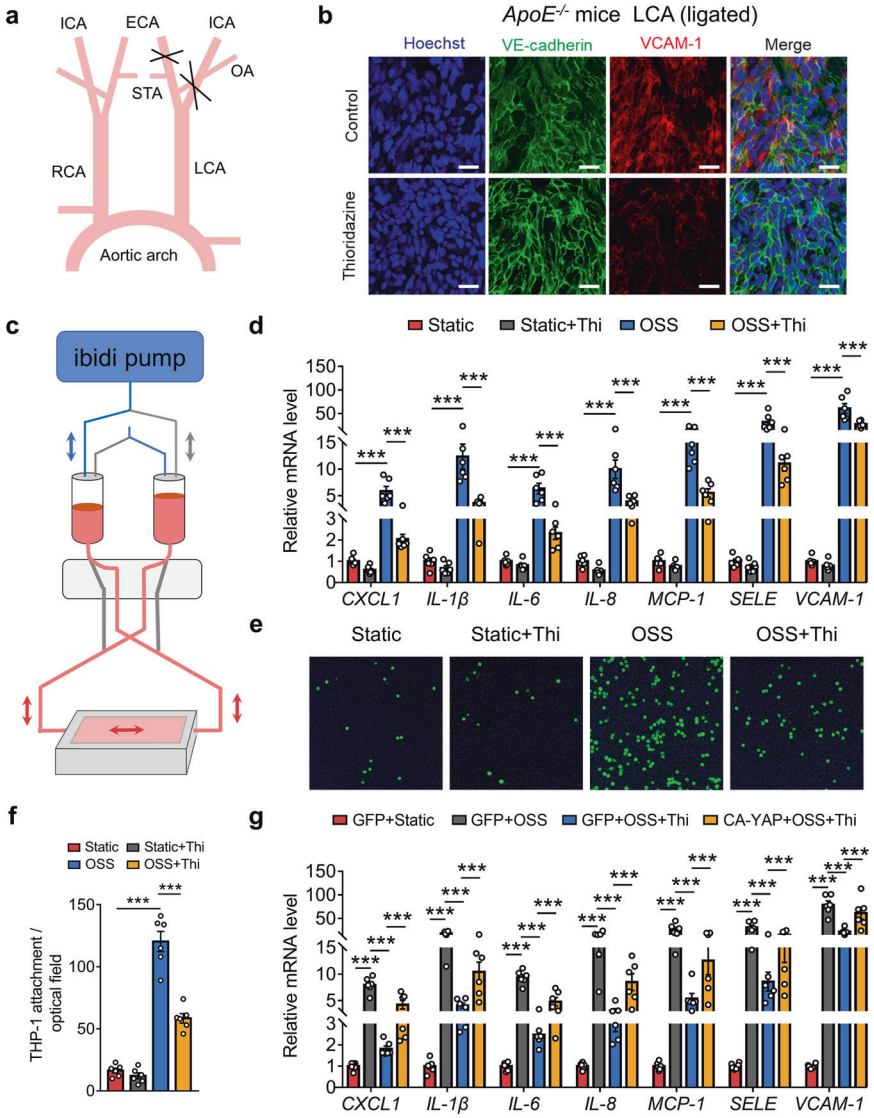

Fig. 3 Thioridazine inhibited disturbed flow-induced endothelial inflammation by restriction of YAP activity. a Schematic diagram showing the surgical strategy for partial ligation of LCA to induce a disturbed flow pattern. **b** *En face* immunofluorescence staining of VCAM-1 in LCA endothelium after two weeks of ligation, scale bar = 20 μm ($n = 4$). **c** Schematic diagram depicting the ibidi flow system for in vitro experiments. **d** HUVECs were subjected to OSS for 4 h after pretreatment of thioridazine (10 μM) or vehicle for 1 h. qRT-PCR results showing the mRNA levels of pro-inflammatory markers (*CXCL1, IL-1β, IL-6, IL-8, MCP-1, SELE, VCAM-1*) ($n = 6$). **e** Representative images of monocytes attaching to HUVECs stimulated by OSS for 6 h ($n = 6$). **f** Quantitative analysis of **e**. **g** HUVECs were transfected with constitutively active YAP for 24 h, followed by thioridazine treatment (10 μM) and OSS for 4 h. qRT-PCR data showing the mRNA levels of pro-inflammatory markers ($n = 6$). Data are presented as means ± SEM. ***$P < 0.001$. ECA External carotid artery, ICA Internal carotid artery, LCA Left common carotid artery, OA Occipital artery, OSS Oscillatory shear stress, STA Superior thyroid artery, RCA Right common carotid artery.

Besides, statins have adverse side effects and clinical contraindications such as statin-associated muscle symptoms, hepatic toxicity, and renal dysfunction [25, 26]. Statin intolerance contributes to discontinuation of statin therapy [26]. Hence, there is still an urgent need to develop more effective therapeutic approaches for atherosclerosis. Previous studies reveal that YAP is a promising therapeutic target for atherosclerosis. Endothelial-specific deletion of YAP mitigated disturbed flow-and western diet-induced atherosclerosis, whereas overexpression of YAP exacerbated atherosclerosis [12, 14, 19]. To search for new YAP inhibitors, we built up the luciferase reporter assay-based drug screening system to screen the FDA-approved drug library. We found that thioridazine potently inhibited the activity of YAP and verified the anti-inflammatory and anti-atherosclerotic effects of thioridazine in vivo and in vitro.

In recent years, some YAP/TAZ inhibitors have been reported in the field of cancer research [27]. Verteporfin and Celastrol were reported to disrupt YAP binding to TEADs in various cancer cell lines [28, 29]. Likewise, peptide mimicking VGLL4 (vestigial-like family member 4) was shown to impair the YAP/TAZ–TEAD interaction, exhibiting anti-tumor therapeutic potential [30, 31]. Song et al. revealed that CA3 potently repressed the expression of YAP1 in esophageal adenocarcinoma cells [32]. Besides, we found that statins suppressed the activity of YAP and TAZ in primary endothelial cells [12]. However, most of the identified compounds and peptides were initially developed for cancer therapy and have not been approved in clinical practice yet. No in vivo evidence indicates their anti-atherosclerotic functions, and their side effects remain to be further elucidated. Some YAP inhibitors, such as verteporfin, exhibit poor water solubility and instability [33], which might restrain their clinical application. Some inhibitors are difficult to synthesize on a large scale in response to clinical demand. Our study proposed the possibility of repurposing thioridazine for anti-

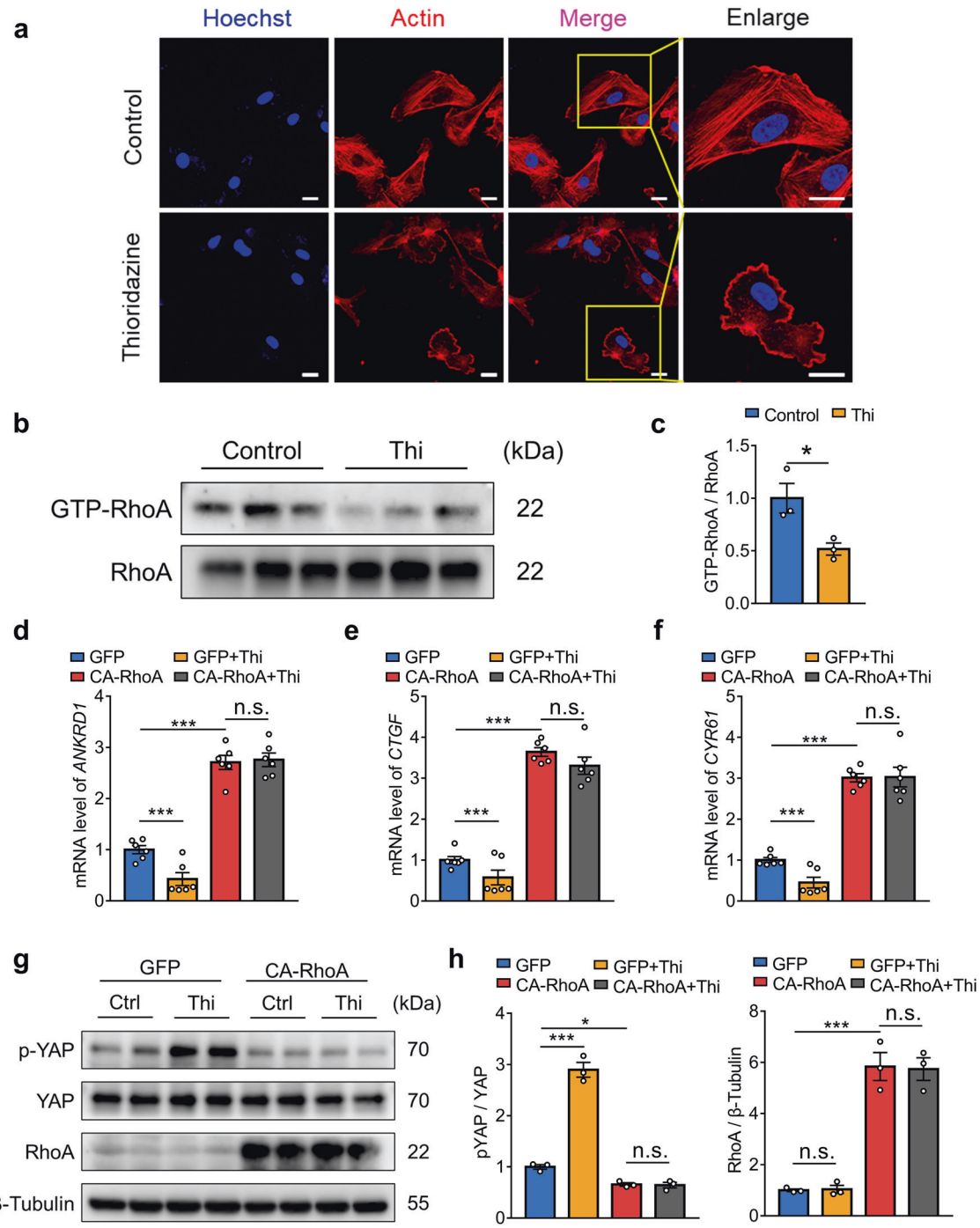

Fig. 4 Thioridazine regulated YAP activity via suppression of RhoA. a, **b** HUVECs were treated with thioridazine or vehicle for 30 min. **a** Cytoskeletal F-actin was stained with phalloidin, scale bar = 20 μm ($n = 4$). **b** GTP-bound RhoA levels were detected by GST-RBD pull-down assay ($n = 3$). **c** Quantitation of the protein level of GTP-RhoA normalized to total RhoA in **b**. **d**–**g** HUVECs were transfected with constitutively active RhoA (Q63L) or negative control plasmids, followed by thioridazine treatment (10 μM) for (**d**–**f**) 4 h and (**g**) 30 min, respectively. **d**–**f** Quantitative real-time PCR analysis on mRNA levels of YAP target genes (*ANKRD1, CTGF, and CYR61*) ($n = 6$). **g** Western blotting on p-YAP (Ser127), total YAP, and RhoA ($n = 3$). **h** Quantitative analysis of **g**. Data are presented as means ± SEM. $^*P < 0.05$, $^{***}P < 0.001$.

atherosclerotic treatment. As an FDA-approved drug, thioridazine might be more suitable for chronic anti-atherosclerotic treatment since its safety profiles are better known than other YAP inhibitors. Repurposing FDA-approved drugs may offer new options and accelerate the development and application of related drugs for anti-atherosclerotic treatment.

Endothelial activation is a principal milestone in the early phase of atherosclerosis process [2, 34]. Atherosclerosis preferentially occurs at curvatures and bifurcations of arteries that are constantly exposed to disturbed flow [35, 36]. As one of the crucial contributors to atherogenesis, disturbed flow impairs endothelial function and triggers endothelial inflammatory response. Previous studies found that disturbed flow activated YAP/TAZ to aggravate endothelial inflammation [12, 14]. In this study, partial ligation mouse model was applied to induce OSS for in vivo experiments, and the ibidi flow system was used to simulate OSS in vitro.

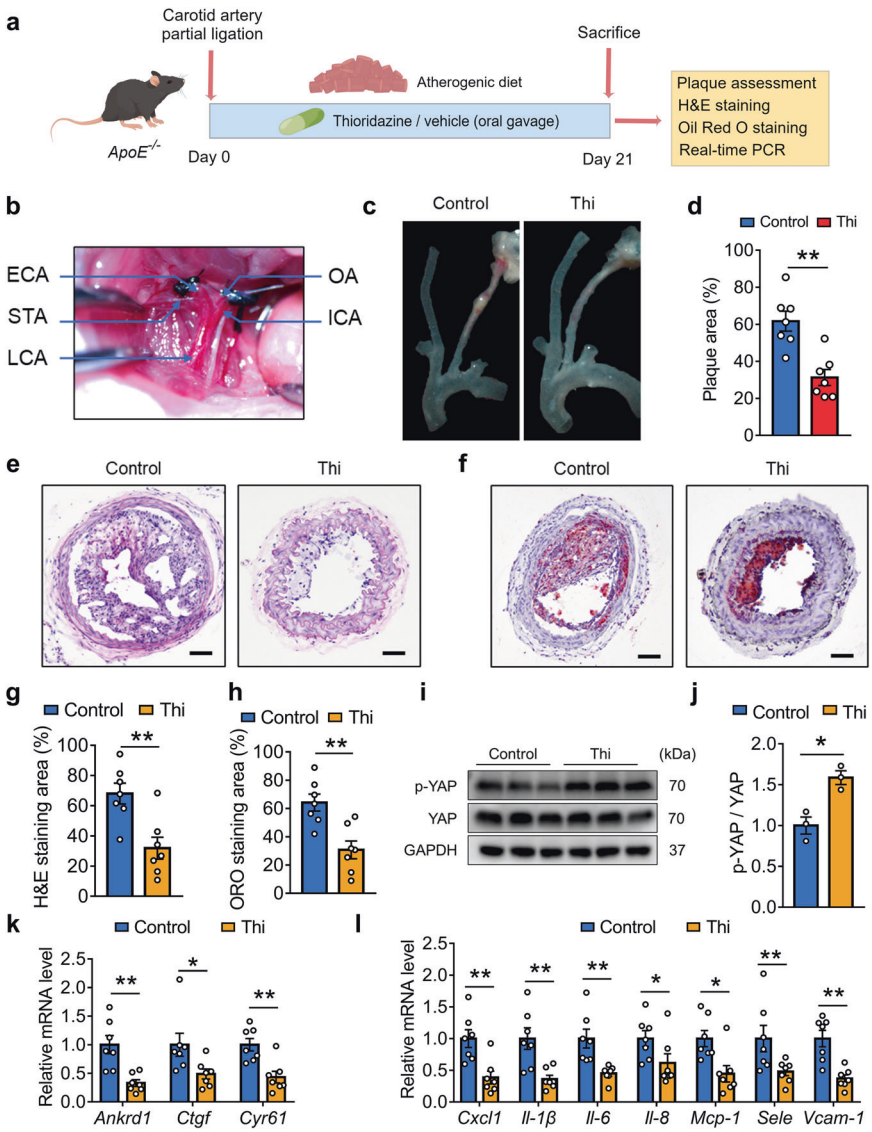

Fig. 5 Oral administration of thioridazine suppressed partial ligation-induced atherogenesis in *ApoE*$^{-/-}$ mice. a The study design for administration of thioridazine on *ApoE*$^{-/-}$ mice. **b** Intraoperative photograph demonstrating the partial ligation of carotid artery in *ApoE*$^{-/-}$ mice. **c** Representative images of the atherosclerotic carotid arteries dissected from *ApoE*$^{-/-}$ mice underwent partial ligation. **d** Quantification of plaque areas in **c**, $n = 7$ per group. **e** H&E staining and **f** Oil Red O staining of the sections of ligated LCA, scale bar = 200 μm. **g, h** Quantitative analysis of **e**, **f** ($n = 7$). **i** Western blotting analysis of p-YAP, YAP in aortas from *ApoE* $^{-/-}$ mice treated with thioridazine. **j** Quantitative analysis of **i. k, l** The relative mRNA levels of *Ankrd1, Ctgf, Cyr61*, and pro-inflammatory markers (*Cxcl1, Il-1β, Il-6, Il-8, Mcp-1, Sele, Vcam-1*) in aortae of the *ApoE*$^{-/-}$ mice were determined by qRT-PCR ($n = 7$). Data are presented as means ± SEM. $^{*}P < 0.05$, $^{**}P < 0.01$ vs control group.

We confirmed that thioridazine inhibited disturbed flow-induced endothelial inflammation in vivo and in vitro. Meanwhile, overexpression of constitutively active YAP abolished the anti-inflammatory effects of thioridazine. This result indicates that thioridazine inhibited endothelial inflammation via restraining YAP. More importantly, the administration of thioridazine mitigated disturbed flow- and high-cholesterol diet-induced atherosclerosis in two *ApoE*$^{-/-}$ mouse models, supporting that YAP is a promising target for atherosclerosis.

The present studies not only identified thioridazine as an atheroprotective YAP inhibitor, but also provided new insight into the molecular mechanism of how thioridazine regulates YAP. The Ras homolog gene family member A (RhoA) is one of the members of Rho family of GTPases. RhoA cycles between an inactive and active conformational state via exchange of GDP and GTP [37]. RhoA plays a prominent role in regulating cytoskeletal dynamics, including the formation of actin stress fibers. RhoA switches its conformational state to regulate a variety of cellular processes [38, 39]. Our study, for the first time, found that thioridazine regulated RhoA activity and cytoskeletal actin dynamics, leading to cell morphological alteration. RhoA has been reported to be involved in the regulation of YAP activity [20–22]. Our previous study identified RhoA as a crucial regulatory factor in the inhibition of YAP/TAZ by laminar flow [12]. Consistently, the present study unveiled that thioridazine suppressed RhoA activity and thus led to YAP cytosol retention and inactivation. Our findings also indicated that targeting RhoA might be a new therapeutic strategy for atherosclerosis, for which further studies are needed.

Previous studies showed that G protein-coupled receptors (GPCRs) are upstream regulators of YAP/TAZ [20]. Consistently, our study also revealed that G protein (Gα13) and integrin β3 interaction regulates YAP phosphorylation in HUVECs [12]. Jie

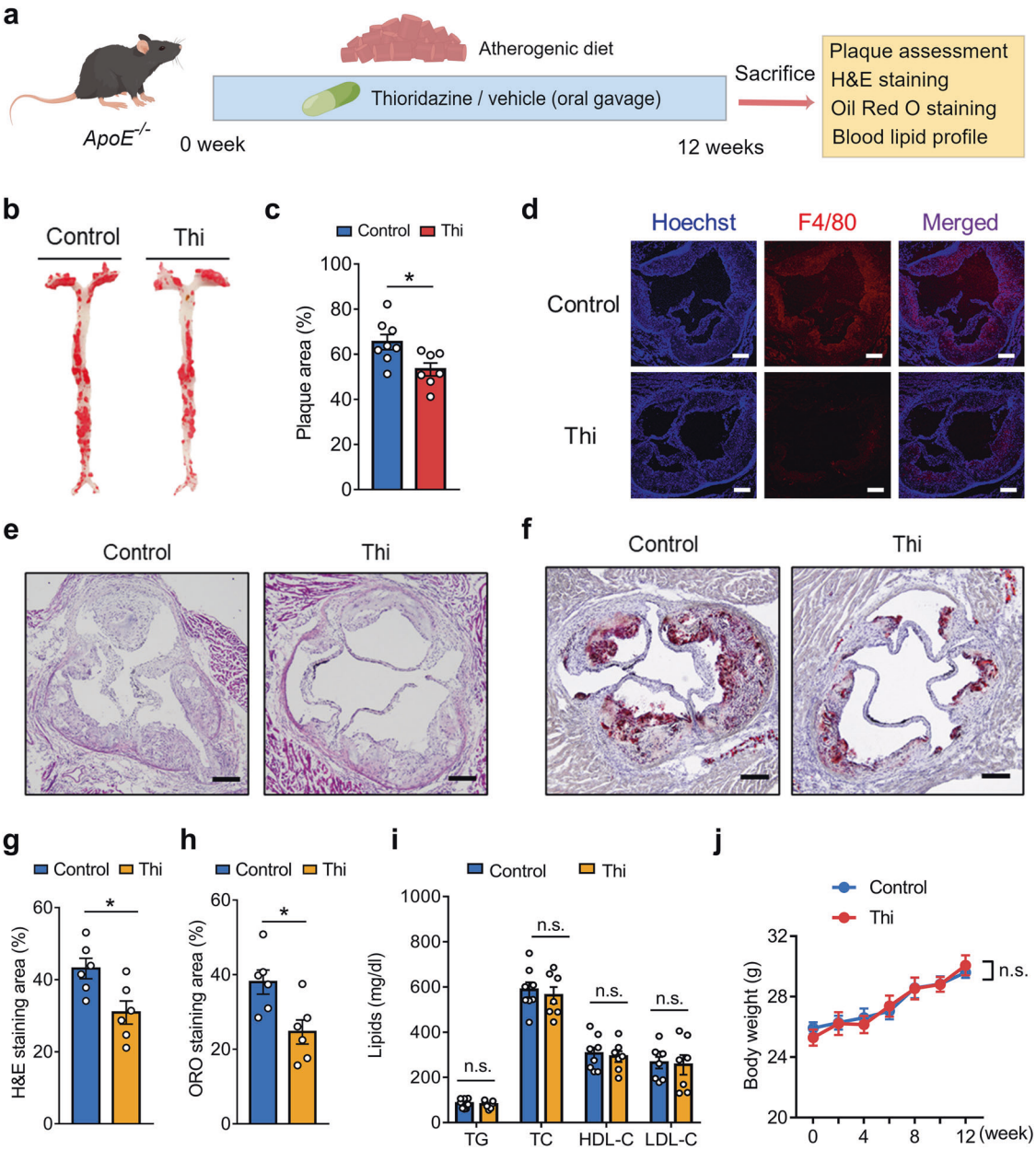

Fig. 6 Chronic thioridazine treatment attenuated high-cholesterol diet-induced atherosclerosis in *ApoE*$^{-/-}$ mice. a The experimental protocol of chronic thioridazine treatment in *ApoE*$^{-/-}$ mice on a high-cholesterol diet. **b** *En face* Oil Red O staining of the aortas. **c** Represents the quantitative analysis result of plaque areas in **b**, $n = 7$ or 8 per group. **d** Immunofluorescent staining of F4/80 in aortic roots. **e** H&E staining, **f** Oil Red O staining of aortic roots, scale bar = 200 μm. **g**, **h** Statistical summary of **e**, **f**, $n = 6$ per group. **i** Lipid profile of the mice, $n = 7$ or 8 per group. **j** Line chart comparing the body weights of the mice. Data are presented as means ± SEM. *$P < 0.05$ vs control group.

Qing et al. reported that an antagonist of dopamine D2 receptor (DRD2), fluphenazine dihydrochloride, blocked YAP activity in macrophages and alleviated liver fibrosis in mice [40]. Thioridazine is widely known as a DRD2 antagonist, implying that DRD2 might be the direct target of thioridazine in endothelial cells. However, in the present study, we found that treatment with DRD2 agonist failed to abrogate the inhibitory effect of YAP by thioridazine in endothelial cells (Supplementary Fig. S4a). Moreover, selective DRD2 antagonists, including domperidone and metoclopramide, cannot inhibit YAP activity in endothelial cells (Supplementary Fig. S4b). These results indicated that thioridazine might not inhibit YAP through DRD2 in endothelial cells. Hence, further studies are required to identify the upstream target that mediates the inhibition of thioridazine on YAP activity in endothelial cells.

Thioridazine belongs to the class of typical phenothiazine antipsychotics, and thus might give rise to weight gain in patients with schizophrenia [41, 42]. In this study, while exhibiting anti-inflammatory and anti-atherosclerotic benefits, thioridazine did not bring about obvious weight gain or alter the lipid profile in *ApoE*$^{-/-}$ mice, possibly due to the low dose of thioridazine administered and these side effects are dose dependent. The adverse effects are mainly due to the functions of thioridazine in the central neural system [41, 43]. It is reasonable to modify the chemical structure of thioridazine to block its penetration of the blood-brain barrier. Employing advanced engineered drug delivery systems might help to achieve therapeutic effects at lower dosages, and even target at the arteries precisely to avoid side effects. Further pharmacokinetic and pharmacodynamic studies of

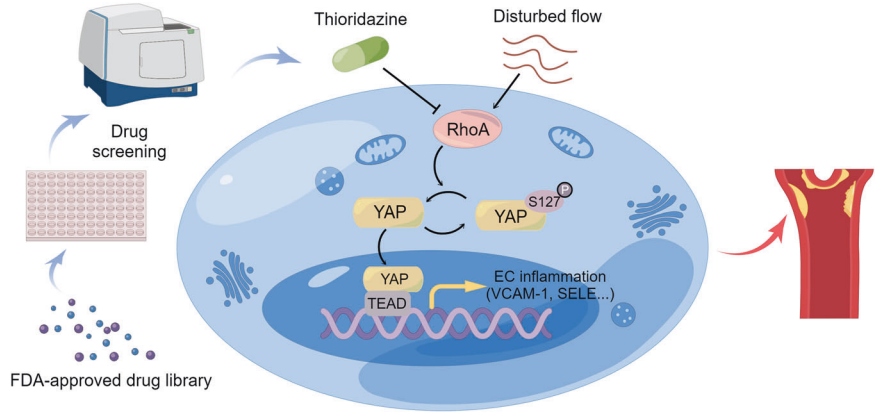

Fig. 7 Schematic overview of repurposing thioridazine for anti-atherosclerotic therapy. Thioridazine was identified as a potent YAP inhibitor by drug screening. Thioridazine inhibits endothelial activation and atherogenesis via suppression of RhoA-YAP axis.

thioridazine in animals are also needed for the prevention of systemic side effects. Previous studies reported the use of thioridazine in cerebral atherosclerosis [44, 45], focusing on the anti-psychotic effects of thioridazine, and whether thioridazine exerted anti-atherosclerotic effects remained unknown. In addition, life expectancy in patients with schizophrenia has been reported to be 15–20 years shorter than the general population, mainly due to an increased risk of cardiovascular diseases [46]. In the present study, we found that thioridazine is not only an anti-psychotic but also an anti-inflammatory and anti-atherosclerotic agent. Hence, thioridazine may be a promising therapeutic option for patients with both atherosclerotic diseases and psychotic disorders, including schizophrenia.

CONCLUSION

To conclude, the present study revealed that the FDA-approved clinical drug thioridazine suppressed endothelial inflammation and atherogenesis through RhoA-YAP signaling pathway. As a novel YAP inhibitor, thioridazine might need further investigation and development for the treatment of atherosclerotic diseases.

ACKNOWLEDGEMENTS

This work was supported by Hong Kong Research Grants Council (SRFS2021-4S04, 14112919, 14164817, 14109720), Hong Kong PhD Fellowship Scheme, and Health and Medical Research Fund (07181286) of China. Schematic diagrams were designed by using Figdraw.

AUTHOR CONTRIBUTIONS

MCJ and HYD designed the study, performed experiments, and analyzed the data. MCJ wrote the manuscript. YHH, CKC, and CWL participated in part of the experiments. YX, XQY, and LW were involved in regular discussion and revised the manuscript. YH designed the study, analyzed the data, wrote the manuscript, provided grant support, and supervised the study. All authors read and approved the submitted manuscript.

ADDITIONAL INFORMATION

Supplementary information The online version contains supplementary material available at https://doi.org/10.1038/s41401-023-01102-w.

Competing interests: The authors declare no competing interests.

REFERENCES

1. Roth GA, Mensah GA, Johnson CO, Addolorato G, Ammirati E, Baddour LM, et al. Global burden of cardiovascular diseases and risk factors, 1990-2019: Update from the GBD 2019 study. J Am Coll Cardiol. 2020;76:2982–3021.
2. Libby P, Buring JE, Badimon L, Hansson GK, Deanfield J, Bittencourt MS, et al. Atherosclerosis. Nat Rev Dis Prim. 2019;5:56.
3. Zhao D. Epidemiological features of cardiovascular disease in Asia. JACC Asia. 2021;1:1–13.
4. Chiu JJ, Chien S. Effects of disturbed flow on vascular endothelium: pathophysiological basis and clinical perspectives. Physiol Rev. 2011;91:327–87.
5. Chatzizisis YS, Coskun AU, Jonas M, Edelman ER, Feldman CL, Stone PH. Role of endothelial shear stress in the natural history of coronary atherosclerosis and vascular remodeling: molecular, cellular, and vascular behavior. J Am Coll Cardiol. 2007;49:2379–93.
6. Kwak BR, Back M, Bochaton-Piallat ML, Caligiuri G, Daemen MJ, Davies PF, et al. Biomechanical factors in atherosclerosis: mechanisms and clinical implications. Eur Heart J. 2014;35:3013–20.
7. Jiang M, Ding H, Huang Y, Wang L. Shear stress and metabolic disorders-two sides of the same plaque. Antioxid Redox Signal. 2022;37:820–41.
8. Ma S, Meng Z, Chen R, Guan KL. The Hippo pathway: biology and pathophysiology. Annu Rev Biochem. 2019;88:577–604.
9. Harvey KF, Zhang X, Thomas DM. The Hippo pathway and human cancer. Nat Rev Cancer. 2013;13:246–57.
10. Reggiani F, Gobbi G, Ciarrocchi A, Sancisi V. YAP and TAZ are not identical twins. Trends Biochem Sci. 2021;46:154–68.
11. Dupont S, Morsut L, Aragona M, Enzo E, Giulitti S, Cordenonsi M, et al. Role of YAP/TAZ in mechanotransduction. Nature. 2011;474:179–83.
12. Wang L, Luo JY, Li B, Tian XY, Chen LJ, Huang Y, et al. Integrin-YAP/TAZ-JNK cascade mediates atheroprotective effect of unidirectional shear flow. Nature. 2016;540:579–82.
13. Yuan P, Hu Q, He X, Long Y, Song X, Wu F, et al. Laminar flow inhibits the Hippo/YAP pathway via autophagy and SIRT1-mediated deacetylation against atherosclerosis. Cell Death Dis. 2020;11:141.
14. Li B, He J, Lv H, Liu Y, Lv X, Zhang C, et al. c-Abl regulates YAPY357 phosphorylation to activate endothelial atherogenic responses to disturbed flow. J Clin Invest. 2019;129:1167–79.
15. Percie du Sert N, Hurst V, Ahluwalia A, Alam S, Avey MT, Baker M, et al. The ARRIVE guidelines 2.0: Updated guidelines for reporting animal research. PLoS Biol. 2020;18:e3000410.
16. Nam D, Ni CW, Rezvan A, Suo J, Budzyn K, Llanos A, et al. Partial carotid ligation is a model of acutely induced disturbed flow, leading to rapid endothelial dysfunction and atherosclerosis. Am J Physiol Heart Circ Physiol. 2009;297:H1535–43.
17. Luo JY, Cheng CK, He L, Pu Y, Zhang Y, Lin X, et al. Endothelial UCP2 is a mechanosensitive suppressor of atherosclerosis. Circ Res. 2022;131:424–41.
18. Shih YT, Wei SY, Chen JH, Wang WL, Wu HY, Wang MC, et al. Vinculin phosphorylation impairs vascular endothelial junctions promoting atherosclerosis. Eur Heart J. 2023;44:304–18.
19. Wang KC, Yeh YT, Nguyen P, Limqueco E, Lopez J, Thorossian S, et al. Flow-dependent YAP/TAZ activities regulate endothelial phenotypes and atherosclerosis. Proc Natl Acad Sci USA. 2016;113:11525–30.
20. Yu FX, Zhao B, Panupinthu N, Jewell JL, Lian I, Wang LH, et al. Regulation of the Hippo-YAP pathway by G-protein-coupled receptor signaling. Cell. 2012;150:780–91.
21. Zhang H, Schaefer A, Wang Y, Hodge RG, Blake DR, Diehl JN, et al. Gain-of-function RHOA mutations promote focal adhesion kinase activation and dependency in diffuse gastric cancer. Cancer Discov. 2020;10:288–305.
22. Tzima E, del Pozo MA, Shattil SJ, Chien S, Schwartz MA. Activation of integrins in endothelial cells by fluid shear stress mediates Rho-dependent cytoskeletal alignment. EMBO J. 2001;20:4639–47.

23. Getz GS, Reardon CA. Animal models of atherosclerosis. Arterioscler Thromb Vasc Biol. 2012;32:1104–15.
24. Sampson UK, Fazio S, Linton MF. Residual cardiovascular risk despite optimal LDL cholesterol reduction with statins: the evidence, etiology, and therapeutic challenges. Curr Atheroscler Rep. 2012;14:1–10.
25. Thompson PD, Panza G, Zaleski A, Taylor B. Statin-associated side effects. J Am Coll Cardiol. 2016;67:2395–410.
26. Bytyci I, Penson PE, Mikhailidis DP, Wong ND, Hernandez AV, Sahebkar A, et al. Prevalence of statin intolerance: a meta-analysis. Eur Heart J. 2022;43:3213–23.
27. Calses PC, Crawford JJ, Lill JR, Dey A. Hippo pathway in cancer: Aberrant regulation and therapeutic opportunities. Trends Cancer. 2019;5:297–307.
28. Wang C, Zhu X, Feng W, Yu Y, Jeong K, Guo W, et al. Verteporfin inhibits YAP function through up-regulating 14-3-3sigma sequestering YAP in the cytoplasm. Am J Cancer Res. 2016;6:27–37.
29. Nouri K, Azad T, Ling M, Janse van Rensburg HJ, Pipchuk A, Shen H, et al. Identification of celastrol as a novel YAP-TEAD inhibitor for cancer therapy by high throughput screening with ultrasensitive YAP/TAZ-TEAD biosensors. Cancers (Basel). 2019;11:1596.
30. Jiao S, Wang H, Shi Z, Dong A, Zhang W, Song X, et al. A peptide mimicking VGLL4 function acts as a YAP antagonist therapy against gastric cancer. Cancer Cell. 2014;25:166–80.
31. Li YW, Xu J, Zhu GY, Huang ZJ, Lu Y, Li XQ, et al. Apigenin suppresses the stem cell-like properties of triple-negative breast cancer cells by inhibiting YAP/TAZ activity. Cell Death Discov. 2018;4:105.
32. Song S, Xie M, Scott AW, Jin J, Ma L, Dong X, et al. A novel Yap1 inhibitor targets CSC-enriched radiation-resistant cells and exerts strong antitumor activity in esophageal adenocarcinoma. Mol Cancer Ther. 2018;17:443–54.
33. Kawamoto R, Nakano N, Ishikawa H, Tashiro E, Nagano W, Sano K, et al. Narciclasine is a novel YAP inhibitor that disturbs interaction between YAP and TEAD4. BBA Adv. 2021;1:100008.
34. Bjorkegren JLM, Lusis AJ. Atherosclerosis: recent developments. Cell. 2022;185:1630–45.
35. Eshtehardi P, McDaniel MC, Suo J, Dhawan SS, Timmins LH, Binongo JN, et al. Association of coronary wall shear stress with atherosclerotic plaque burden, composition, and distribution in patients with coronary artery disease. J Am Heart Assoc. 2012;1:e002543.
36. Morbiducci U, Kok AM, Kwak BR, Stone PH, Steinman DA, Wentzel JJ. Atherosclerosis at arterial bifurcations: evidence for the role of haemodynamics and geometry. Thromb Haemost. 2016;115:484–92.
37. Shimokawa H, Sunamura S, Satoh K. RhoA/Rho-kinase in the cardiovascular system. Circ Res. 2016;118:352–66.
38. Eckenstaler R, Hauke M, Benndorf RA. A current overview of RhoA, RhoB, and RhoC functions in vascular biology and pathology. Biochem Pharmacol. 2022;206:115321.
39. Shimokawa H, Satoh K. 2015 ATVB plenary lecture: translational research on rho-kinase in cardiovascular medicine. Arterioscler Thromb Vasc Biol. 2015;35:1756–69.
40. Qing J, Ren Y, Zhang Y, Yan M, Zhang H, Wu D, et al. Dopamine receptor D2 antagonism normalizes profibrotic macrophage-endothelial crosstalk in non-alcoholic steatohepatitis. J Hepatol. 2022;76:394–406.
41. Dayabandara M, Hanwella R, Ratnatunga S, Seneviratne S, Suraweera C, de Silva VA. Antipsychotic-associated weight gain: management strategies and impact on treatment adherence. Neuropsychiatr Dis Treat. 2017;13:2231–41.
42. Varga B, Csonka A, Csonka A, Molnar J, Amaral L, Spengler G. Possible biological and clinical applications of phenothiazines. Anticancer Res. 2017;37:5983–93.
43. Raben AT, Marshe VS, Chintoh A, Gorbovskaya I, Muller DJ, Hahn MK. The complex relationship between antipsychotic-induced weight gain and therapeutic benefits: a systematic review and implications for treatment. Front Neurosci. 2017;11:741.
44. Predescu V, Ciurezu T, Nica S, Ionescu R, Tudorache D, Niturad A, et al. Utilization of thioridazine combined with hydergine in the treatment of incipient mental disturbances in cerebral atherosclerosis. Rev Roum Neurol Psychiatr. 1974;11:243–8.
45. Vallet R. Treatment of psychic disorders of cerebral atherosclerosis: diagnostic, nosologic and pathogenic aspects. Ann Med Psychol (Paris). 1964;122:515–41.
46. Veeneman RR, Vermeulen JM, Abdellaoui A, Sanderson E, Wootton RE, Tadros R, et al. Exploring the relationship between schizophrenia and cardiovascular disease: a genetic correlation and multivariable Mendelian randomization study. Schizophr Bull. 2022;48:463–73.